Letter

Engineering the optical absorption in S-hyperdoped Si from short wavelength to far infrared: A first-principles study

Francesco Melone
CNR-IMM, sede Agrate Brianza, via Olivetti 2, I-20864 Agrate Brianza, Italy
and Dipartimento di Fisica "Aldo Pontremoli," Universitá degli Studi di Milano, via Celoria 16, I-20133 Milano, Italy

Giovanni Onida
Dipartimento di Fisica "Aldo Pontremoli," Universitá degli Studi di Milano, via Celoria 16, I-20133 Milano, Italy
and INFN, Sezione di Milano, via Celoria 16, I-20133 Milano, Italy

Alberto Debernardi*
CNR-IMM, sede Agrate Brianza, via Olivetti 2, I-20864 Agrate Brianza, Italy

(Received 5 September 2024; accepted 9 April 2026; published 11 May 2026)

By combining Density functional theory-based first-principles simulations with a random distribution model for estimating the relative percentage of distinct types of S complexes in S-hyperdoped silicon, we predict a tunability of the insulator-to-metal transition at the critical dopant concentration that is significantly larger than previously reported for other chalcogen-hyperdoped Si systems, driven by the relative abundance of the different complexes. By assuming the possibility to tune the latter during the sample synthesis, we predict that optical absorption spectra of S-hyperdoped Si can be engineered from the short wavelength infrared to far infrared region.

DOI: 10.1103/y5zw-qt7d

Hyperdoping, i.e., doping a material beyond the solid solubility limit, is a recently developed experimental technique that allows one to achieve unprecedented dopant concentrations (x) in semiconductors, while keeping the crystalline structure of the host material.

In general, the introduction of dopant generates impurity levels in the semiconductor band gap that, as the dopant concentration increases, form an impurity band (IB). The IB width increases for increasing x, due to the increase of the overlap of dopant wave functions—corresponding to shallow electronic states—as the average distance between the dopants, randomly distributed in the crystal, decreases. The critical concentration, x_c, at which the IB merges into the conduction band (CB) corresponds to the Insulator-to-Metal transition (IMT) [1,2].

The presence of IB whose width can be tuned by the dopant concentration has been at the origin of several proposals for the exploitation of hyperdoped semiconductors, ranging from intermediate band photovoltaics [3,4], to infrared sensors [5–7], to nanoelectronics [8–11].

Silicon, for its earth abundance, well-established technology, and large employment in the semiconductor industry, constitutes the ideal candidate as the host material for hyperdoping.

Among Si dopants, chalcogens, i.e., elements of group VI of the periodic table, are attracting significant interest because their electron concentration increases monotonically as the doping concentration increases [12]. At variance, group V dopants, commonly employed in Si, show carrier saturation at a dopant concentration $\sim$8–10 $\times$ 10^{20} [8]. In particular, a Te concentration of as high as 2.5 at. % ($\sim$1.25 $\times$ 10^{21} cm^{-3}) [8,9], thus exceeding one electron per nm^{-3}, has been reached in hyperdoped Si without showing any sign of saturation, paving the way to ultrascaled nanoelectronics.

However, the high dopant concentration promotes the formation of different types of complexes [13]. Since the population of each type of complex influences the electronic and optical properties of the system, a crucial role is played by theory, and, in particular, by first-principles calculations, in order to understand the physical properties of such hyperdoped semiconductors. In Refs. [8,10], for example, the role played by Te or Se dimers and by other complexes in the nonsaturating free-electron density of chalcogen-hyperdoped Si has been studied, revealing the impurity complexes responsible for the electrical behaviors in both Te- and Se-hyperdoped Si [8–11]. Furthermore, the complexes formed by a Si vacancy surrounded by four (three) adjacent substitutional chalcogens have been predicted by first principles [10,11,14] and then experimentally detected [15,16].

In the present work, we analyze the case of Sulfur, the element preceding Se and Te in the chalcogen group.

In experimental procedures aimed at synthesizing hyperdoped silicon samples, dopants such as sulfur (S), selenium

*Contact author: alberto.debernardi@cnr.it

(Se), or tellurium (Te) are initially introduced into the silicon matrix, typically via ion implantation. Subsequently, pulsed laser melting epitaxy (PLME) is employed to locally melt the doped surface layer. This technique enables epitaxial recrystallization, with the solidification front propagating from the bottom of the molten region toward the surface at velocities of several meters per second.

In the context of conventional doping techniques, the diffusion behavior of sulfur in silicon is commonly interpreted through a model involving interstitial (S_i)–substitutional (S_{Si}) exchange, which may occur via the simultaneous participation of silicon self-interstitials (Si_i) and vacancies (V_{Si}) [17–19]. However, in our case, due to the rapid nature of the epitaxial regrowth process, dopants do not have sufficient time to diffuse and reach their equilibrium configuration, which would otherwise result in phase separation. Instead, their diffusion is strongly suppressed.

The peculiar mechanisms governing dopant diffusion under these specific conditions remain not fully understood. Nevertheless, they can be phenomenologically described by the model proposed in Refs. [10,11], where the characteristic diffusion length is denoted by Λ_d. As in the cases of selenium and tellurium, the population of sulfur-related complexes can be estimated using a statistical model [11] based on the random distribution of dopants over the lattice sites of the host crystal. Let N_{Si} and N_S denote the number of silicon and sulfur atoms in the supercell (or, equivalently, in the sample), respectively. The probability that a lattice site is occupied by a sulfur atom is given by

$$x = \frac{N_S}{N_S + N_{Si}}.$$

We assume that n sulfur atoms can form a point defect or a complex D_n (with n being the number of sulfur atoms involved) if $n-1$ of them are located within the Λ_dth coordination shell surrounding a central sulfur atom. The parameter Λ_d is a positive integer [20] representing the effective diffusion length of dopants during the recrystallization process. This length is expected to depend on the specific experimental conditions—such as temperature, pulse duration, and laser fluence—typically employed during pulsed or flash laser annealing [7] following ion implantation.

Consequently, a larger dopant diffusion length within the crystal corresponds to a higher value of Λ_d, thereby increasing the likelihood of forming larger sulfur complexes.

The relative concentration of different types of complexes can be evaluated using the model introduced in Ref. [10], where dopants are randomly distributed according to a binomial distribution [21],

$$p_{m+1}(x) = \binom{N_{\Lambda_d}}{m} x^m (1-x)^{N_{\Lambda_d}-m}, \tag{1}$$

where $N_{\Lambda_d} \equiv \sum_{k=1}^{\Lambda_d} z_k$ is the total number of lattice sites within the Λ_dth shell, and z_k denotes the number of sites in the kth shell.

The probability associated with a complex D_n, composed of n sulfur atoms with m dopants located within the Λ_dth shell, is given by

$$p_m^{D_n}(x) = \frac{p_m(x)}{Z_m}\, e^{-E_{D_n}^{\mathrm{form}}(x)/k_B T}\, \Theta(m-n), \tag{2}$$

where $E_{D_n}^{\mathrm{form}}$ is the formation energy of the defect D_n, T is the temperature, k_B is the Boltzmann constant, and $\Theta(x)$ is the Heaviside step function.

The partition function Z_m is defined as

$$Z_m \equiv \sum_{D_n}^{n \leqslant m} e^{-E_{D_n}^{\mathrm{form}}(x)/k_B T}, \tag{3}$$

where the sum runs over all distinct defect types D_n with $n \leqslant m$.

Finally, the total probability of forming a defect D_n is given by

$$p^{D_n}(x) = \sum_m p_m^{D_n}(x). \tag{4}$$

Note*:* Since the binomial distribution inherently accounts for the various possible configurations of dopants in adjacent lattice sites, the contribution of configurational entropy is neglected to avoid double counting.

Key ingredients are hence the formation energies $E_{D_n}^{\mathrm{form}}(x)$. The latter can be reliably estimated by *ab initio* calculations based on Density Functional Theory within the supercell approach. Giving a complex D and a sulfur concentration x, the formation energy of D per S atom is

$$E_D^{\mathrm{form}}(x) = [E_D(x) - N_{Si}\mu_{Si} - N_S\mu_S]/N_S, \tag{5}$$

where $E_D(x)$ is the total energy of the supercell containing the defect D, μ_{Si} is the chemical potential of bulk silicon and μ_S is the chemical potential of S in bulk silicon disulfide, SiS_2, at equilibrium with bulk Si.

We considered different types of S complexes: the monomer, S_{Si}, is a substitutional S in the host lattice site; the dimer, $S_{Si}S_{Si}$, with two substitutional S in the nearest-neighbor lattice sites; the interstitials, S_i^{tet} and S_i^{hex}, with the S interstitial at the tetrahedral or hexagonal position, respectively; the complex formed by a Si vacancy having in the nearest-neighboring lattice sites n substitutional sulfurs, VS_n ($n = 1, 2, 3, 4$) [22].

All defect configurations are treated as neutral, consistently with the hyperdoped regime where the Fermi level lies close to or above the conduction-band minimum, making neutral charge states energetically favored [see Supplemental Material (SM) [23]].

In Fig. 1 we display the formation energy of distinct types of complexes as a function of S concentration. The curves are qualitatively similar, increasing with S concentration until x reaches a value $\in [0.5\%, 1\%]$ and then being essentially independent of x [24]. The difference in formation energy between the S_{Si} monomer and the S_{Si}-S_{Si} dimer is consistent with the value reported in Ref. [19], obtained using the local density approximation.

The complexes with the smaller formation energies are $S_{Si}S_{Si}$, VS_3, and VS_4, but they are also those involving the larger number of S atoms, so their relative frequency in a realistic crystal is highly dependent on the probability of having enough S atoms to form the complex.

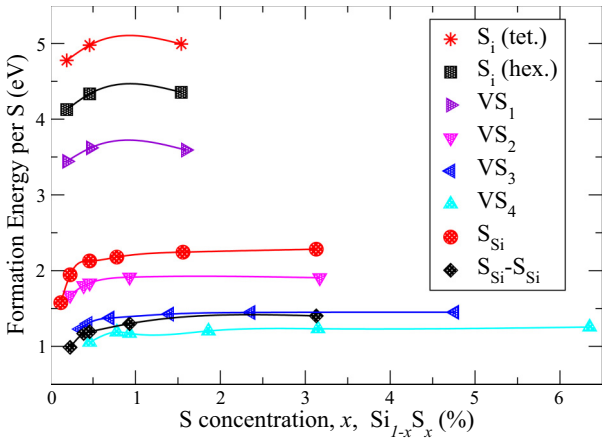

FIG. 1. Formation energy (per S atom) of different types of S complexes in Si:S. Symbols denote first-principles data; solid lines are obtained by normal cubic spline interpolation.

On the other hand, S_i(tet), S_i(hex), and VS_1 demand only one atom of sulfur, but the large formation energy of the three, exceeding by 1 eV or more the one of S_{Si} monomer, make them very unlikely to form. The formation of S_{Si} is then favored, making it one of the most frequent complexes. Note that at variance with the case of Se-hyperdoped Si [10], in Si:S the $S_{Si}S_{Si}$ dimer has a lower formation energy than VS_3, thus promoting the formation of the $S_{Si}S_{Si}$ dimer and VS_4. The complexes considered in the computation of their formation probabilities—and thus of their contributions to the electronic and optical properties of S-hyperdoped Si—are those exhibiting the lowest formation energies, namely, S_{Si}, $S_{Si}S_{Si}$, VS_2, VS_3, and VS_4. Their formation energies are more than 1 eV lower than those of the neglected complexes.

The results for four different values of the diffusion length Λ_d are shown in Fig. 2. To evaluate these relative concentrations, we set the temperature to $T = 1687$ K, corresponding to the melting point of silicon (see also Refs. [10,11]). The probabilities are computed using a Boltzmann distribution that accounts for both the formation energies and the configurational degeneracies of the complexes.

With the only exception of the monotonically decreasing $p^{S_{Si}}(x)$, all the probabilities to form complexes of type D increase up to a concentration of dopant $x = \upsilon^D(\Lambda_d)$ and then start decreasing, with $\upsilon^{S_{Si}\text{-}S_{Si}}(\Lambda_d) < \upsilon^{VS_3}(\Lambda_d) < \upsilon^{VS_4}(\Lambda_d)$. In general, for each D we have $\upsilon^D(\Lambda_{d2}) < \upsilon^D(\Lambda_{d1})$ when $\Lambda_{d2} > \Lambda_{d1}$.

The electronic properties of each type of S complex are determined by the position and width of the IB they form within the gap between the valence band (VB) and the CB of bulk Si.

To compare their behaviors, in Fig. 3 we display the Density of States (DOS) of the electronic band structure at $x \sim 0.46$ at. %. This choice of concentration allows us to compute by the supercell approach the DOS of different complexes at (approximately) the same concentrations x close to the IMT.

Starting from the complexes with a higher formation energy, S_i(tet) is a shallow double-acceptor defect, where its IB is in the Si band gap close to the VB maximum; S_i(hex) possesses a metallic IB relatively deep in the band gap and

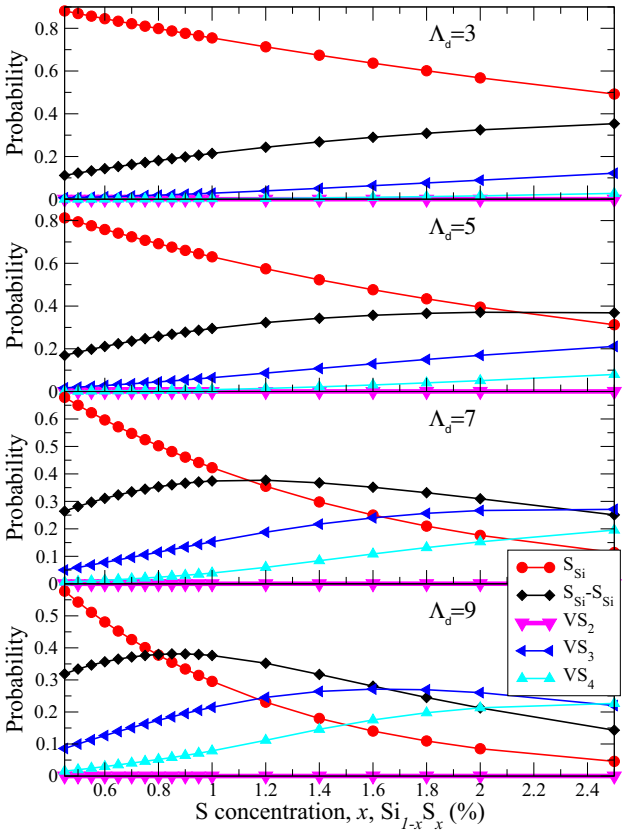

FIG. 2. Calculated probabilities of various sulfur defect complexes as a function of sulfur concentration, for different values of the diffusion length $\Lambda_d = 3, 5, 7, 9$ (see text).

therefore it can act as a deactivation center for the electrons in impurity states of higher energy or in the CB; VS_1 and VS_2 have a metallic IB, occupied by two electrons, that is almost (VS_1) or already (VS_2) merged with the CB, and thus both the two complexes are double donors. Note that VS_1 (VS_2) behaves as S_{Si} ($S_{Si}S_{Si}$) providing two electrons per complex to CB.

The DOS of S_{Si} and $S_{Si}S_{Si}$ are characterized by an insulating IB filled by two electrons, thus, each complex is a double donor (i.e., one S provides two electrons to the CB if assembled in S_{Si}, while it provides one electron to the CB if

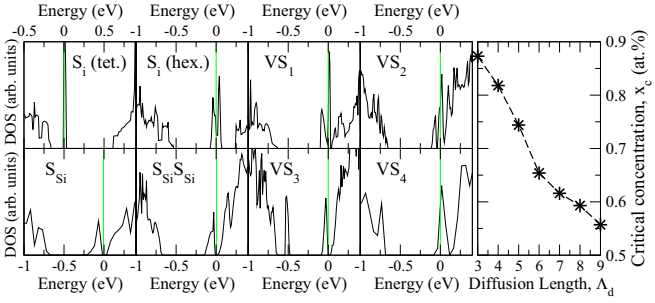

FIG. 3. Left/middle panels: Density of States for different S complexes at $x = 0.46$ at. %. The green vertical line highlights the Fermi Energy. Right panel: Critical concentration of the Insulator-to-Metal Transition as a function of diffusion length Λ_d.

assembled in $S_{Si}S_{Si}$, thus forming a double bond between the two S's), with $S_{Si}S_{Si}$ forming a shallower IB than S_{Si}.

VS_3 possesses two IB: one near the top of the VB, the lower impurity band (LIB), and one overlapped with the CB, the higher impurity band (HIB). Both the LIB and the HIB are occupied by two electrons. The double IB structure, already observed for the analogous complex in Se-hyperdoped Silicon [10], brings more electronic states for subthreshold photon absorption, and therefore it is a promising feature for Si-based midinfrared detection. Finally, VS_4 has a shallow metallic IB populated by four electrons.

The analysis above, despite being limited to the $x \simeq 0.46$ at. %, provides a starting point to predict the DOS of the eight complexes with different S concentrations, knowing that increasing (or decreasing) the concentration has the effect of increasing (or decreasing) the width of the IB up to the point where the IB merges with (or splits from) the CB.

Following Ref. [10], for each complex D, naming x the doping concentration and x_M as the value at which the IB maximum overlaps with the CB minimum, we can distinguish two ranges: the interaction range, where x, although being sufficiently high for the impurities to interact with each other, remains smaller than x_M, so that an increase of x induces a broadening of the IB, and the metallic range, with $x \geqslant x_M$, where the IB is merged to the conduction band.

The formation energy of different complexes, together with the electronic structures discussed above, explain the nonsaturating free-electron density experimentally detected in sulfur-hyperdoped Si [12], because the deactivation complexes rarely form.

To rigorously account for the coexistence of several sulfur complexes full multidefect calculations would be necessary, requiring extremely large supercells which are completely out of reach within our *ab initio* approach. Our calculations, instead, rigorously describe an experimental situation where a single type of complex predominates. However, a phenomenological interpolation scheme, based on some kind of averaging, may be used to go beyond that case and to derive a rough estimate of effective critical concentrations in cases where several sulfur complexes coexist. For example, the approximate model previously proposed by some of us [10,11] uses a harmonic-mean estimator, which is conceived in order to yield values of $\bar{x}_c$ bounded between the smallest and largest single-complex thresholds, completely neglecting cross-interactions [25],

$$\frac{1}{\bar{x}_c(x)} = \sum_{D_n} \frac{c_{D_n}(x)}{x_M(D_n)}, \quad \bar{x}_c(x_c) = x_c, \tag{6}$$

where $c_{D_n}(x)$ is the fraction of S atoms in complexes D_n, and $x_M(D_n)$ is the threshold for defect type D_n marking the merging of its impurity band with the CB. Such thresholds represent hence well-defined limiting cases in the single-complex approximation. By using $x_M(S_{Si}) = 2$ at. %, $x_M(S_{Si}S_{Si}) = 0.46$ at. %, $x_M(VS_3) = 0.35$ at. %, and $x_M(VS_4) = 0.50$ at. %, one gets the estimate for the variation of x_c with Λ_d shown in the rightmost panel of Fig. 3. Despite the roughness of the model, the critical concentration at which the IMT occurs decreases with increasing Λ_d, as expected, since the increase of dopant diffusion increases the probability to form complexes involving more than one S, thus reducing the percentage of S_{Si} monomer which is the complex type having the highest x_M [note that $x_M(S_{Si})$ is more than four times greater than the other x_M].

TABLE I. Energy of the absorption maximum peak (AMP) and its full width half maximum (FWHM) of the optical spectra of the S_{Si} and of the most probable pairs of complexes.

Complexes	S (at. %)	AMP (eV)	IR-AMP	FWHM (eV)
S_{Si}	1.56	0.464	SWIR	0.606
S_{Si}-$S_{Si}S_{Si}$	1.17	0.165	MWIR	0.486
$S_{Si}S_{Si}$-VS_3	1.96	0.111	LWIR	0.285
$S_{Si}S_{Si}$-VS_4	2.35	0.111	LWIR	0.285
S_{Si}-VS_4	1.96	0.099	LWIR	0.303
S_{Si}-VS_3	1.57	0.083	FIR-LWIR	0.254

Therefore, a tuning of the relative concentrations of distinct types of complexes may allow the engineering of IMT with a variation of Δx_c of the order of 36% or more, according to the variation of the parameter Λ_d that in our model represents the mobility of dopants during the synthesis process of hyperdoped Si. Note that, by considering Si containing only S_{Si}, where $x_c = 2$ at. %, Δx_c exceeds 70%. The critical concentration of Se-hyperdoped Si [11], instead, varies only of 4% in the same interval of $\Lambda_d \in [3, 9]$, thus suggesting an unprecedented tunability of IMT in S-hyperdoped Si [26].

The possibility to tune the relative percentage of distinct types of complexes formed by S in hyperdoped Si, has important consequences to the absorption spectra of the material, as illustrated below.

The simulation of the imaginary part of the dielectric function, $\epsilon(\omega)$, directly related to the optical absorption spectra [27], provides reliable predictions of the efficiency of S-hyperdoped Si to absorb and detect photons in the infrared (IR) region of the electromagnetic spectra. To investigate the optical properties of S-hyperdoped Si, we computed $\mathrm{Im}[\epsilon(\omega)]$ within the G_0W_0 approximation, using the plasmon-pole model and including local field effects (see SM for further methodological information, which includes Refs. [28–40]). S concentrations are chosen in the range $x \in [1.17, 2.35]$ at. %, representing a reasonable compromise between a computationally affordable supercell size and concentrations close to the IMT. We considered the IR spectra of S_{Si} monomers ($x =$ 1.56 at. %) and of the most probable pairs of different S complexes that can be obtained as Λ_d varies, namely S_{Si}-$S_{Si}S_{Si}$ ($x = 1.17$ at. %), S_{Si}-VS_3 ($x = 1.57$ at. %), $S_{Si}S_{Si}$-VS_3 ($x =$ 1.96 at. %), S_{Si}-VS_4 ($x = 1.96$ at. %), and $S_{Si}S_{Si}$-VS_4 ($x =$ 2.35 at. %); the results are represented in Fig. 4. In view of applications such as IR detector we focused our study on the absorption spectra within the bulk Si band gap up to 1.1 eV. The relevant parameters describing each spectrum are summarized in Table I.

For small Λ_d value, the monomers S_{Si} represent the large majority of S complexes. In fact, in the limiting case in which the dopants do not diffuse and remain located at the lattice sites according to the binomial distribution [Eq. (1)], the prob-

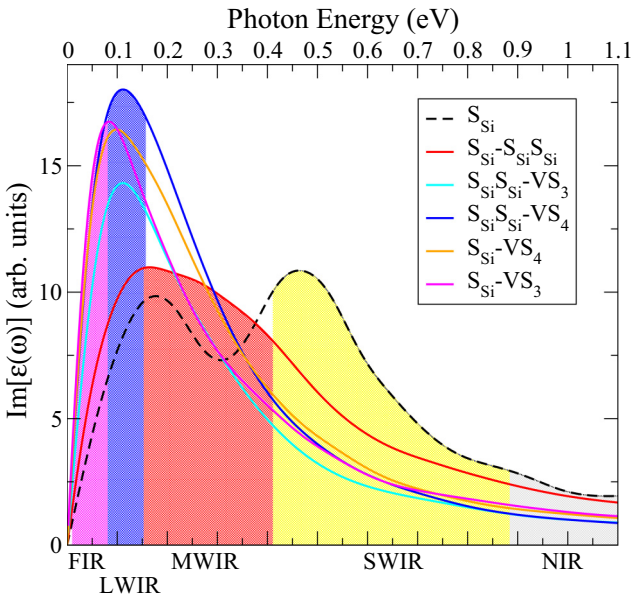

FIG. 4. Optical spectra due to different combination of S complexes in hyperdoped Si. The spectra are normalized to the S concentration for comparison. For the low-symmetry complexes VS_3, spectra are averaged over Cartesian directions.

ability of finding an isolated S is more than 90% for $x \leqslant 2.5\%$, i.e., the dopant population is almost fully constituted by S monomer.

For the S_{Si} monomer, in the IR region, the Im[$\epsilon(\omega)$] has the main peak at 0.464 eV, in the Short-Wavelength IR (SWIR) region (the lower bond of the near SWIR range is 0.413 eV), consistently with the broad absorption band which peaks at around 0.4–0.5 eV measured in S-hyperdoped Si [12]. In Fig. 4, a secondary absorption peak appears at approximately 0.177 eV, close to the transition between the long-wavelength infrared (LWIR) and midwavelength infrared (MWIR) regions.

This situation is radically changed if other types of S complexes are present in a significant amount. For example, for $\Lambda_d = 5$ and $x \sim 2$ at. % (Fig. 2), S_{Si} monomers and $S_{Si}S_{Si}$ dimers are equally probable, and together constitute the ∼80% of S complexes. The presence of S_{Si}-$S_{Si}S_{Si}$ pairs produces a significant redshift of the absorption peak, as can be noticed in Fig. 4, where the corresponding Im[$\epsilon(\omega)$] presents a maximum at 0.165 eV in the MWIR.

Significantly, the relative percentage of VS_3 and VS_4 increases as Λ_d increases, so the main peak of the absorption spectrum further redshifts. In fact, the computed Im[$\epsilon(\omega)$] for S_{Si}-VS_4, $S_{Si}S_{Si}$-VS_3, and $S_{Si}S_{Si}$-VS_4 show peaks in Long-Wavelength IR (LWIR), while for S_{Si}-VS_3 the peak is at 83 meV, i.e., at the limit between the Far-IR (FIR) and LWIR region (83 meV). In general, for every system composed of two distinct types of S complexes, the Full Width at Half Maximum of the absorption peak decreases as the peak position shifts to lower energies.

In chalcogen-hyperdoped Si, the tailoring of IR absorption is commonly achieved by increasing the dopant concentration, thus broadening the IB peak, to tune the gap between the CB minimum and the Fermi energy within the IB [2,7].

Our results suggest that it is possible to engineer IR absorption *at a given dopant concentration* by modifying the *relative percentage* of distinct types of complexes by acting to the diffusion length Λ_d during the sample synthesis. This characteristic is related to the tunability of the IMT that, in Si hyperdoped with S, is significantly higher than the one predicted for Se doping in the same range of Λ_d. Similar trends are also expected at lower concentration x and higher Λ_d.

In summary, by first-principles simulations, we enlighten the microscopic mechanisms responsible for the IMT in S-hyperdoped Si, showing a tunability of the critical concentration that, in Λ_d range we investigated, exceeds 35%. Furthermore, the Im[$\epsilon(\omega)$] computed for the more common types of S complexes reveals the possibility to engineer the optical absorption from SWIR to FIR by tailoring the *relative percentage* of distinct types S complexes, while the S concentration is kept fixed.

Our results suggest S-hyperdoped Si as an ideal candidate building block material for the next generation of IR photodetector and nanometer-sized electronic devices.

We acknowledge the CINECA award under the ISCRA initiative, for the availability of high-performance computing resources and support (MaCHD-Si project), and R. Colnaghi for technical support on the computer hardware.

[1] M. T. Winkler, D. Recht, M.-J. Sher, A. J. Said, E. Mazur, and M. J. Aziz, Insulator-to-metal transition in sulfur-doped silicon, Phys. Rev. Lett. **106**, 178701 (2011).

[2] E. Ertekin, M. T. Winkler, D. Recht, A. J. Said, M. J. Aziz, T. Buonassisi, and J. C. Grossman, Insulator-to-metal transition in selenium-hyperdoped silicon: Observation and origin, Phys. Rev. Lett. **108**, 026401 (2012).

[3] A. Luque, A. Marti, and C. Stanley, Understanding intermediate-band solar cells, Nat. Photon. **6**, 146 (2012).

[4] Y. Okada, N. J. Ekins-Daukes, T. Kita, R. Tamaki, M. Yoshida, A. Pusch, O. Hess, C. C. Phillips, D. J. Farrell, K. Yoshida, N. Ahsan, Y. Shoji, T. Sogabe, and J. F. Guillemoles, Intermediate band solar cells: Recent progress and future directions, Appl. Phys. Rev. **2**, 021302 (2015).

[5] S. Hu, P. Han, S. Wang, X. Mao, X. Li, and L. Gao, Improved photoresponse characteristics in Se-doped Si photodiodes fabricated using picosecond pulsed laser mixing, Semicond. Sci. Technol. **27**, 102002 (2012).

[6] Y. Berencén, S. Prucnal, F. Liu, I. Skorupa, R. Huebner, L. Rebohle, S. Zhou, H. Schneider, M. Helm, and W. Skorupa, Room-temperature short-wavelength infrared Si photodetector, Sci. Rep. **7**, 43688 (2017).

[7] M. Wang and Y. Berencén, Room-temperature infrared photoresponse from ion beam–hyperdoped silicon, Phys. Status Solidi A **218**, 2000260 (2021).

[8] M. Wang, A. Debernardi, Y. Berencén, R. Heller, C. Xu, Y. Yuan, Y. Xie, R. Böttger, L. Rebohle, W. Skorupa, M. Helm, S. Prucnal, and S. Zhou, Breaking the doping limit

in silicon by deep impurities, Phys. Rev. Appl. **11**, 054039 (2019).

[9] M. Wang, A. Debernardi, W. Zhang, C. Xu, Y. Yuan, Y. Xie, Y. Berencén, S. Prucnal, M. Helm, and S. Zhou, Critical behavior of the insulator-to-metal transition in Te-hyperdoped Si, Phys. Rev. B **102**, 085204 (2020).

[10] A. Debernardi, First principles simulations of microscopic mechanisms responsible for the drastic reduction of electrical deactivation defects in Se hyperdoped silicon, Phys. Chem. Chem. Phys. **23**, 24699 (2021).

[11] A. Debernardi, Engineering the insulator-to-metal transition by tuning the population of dopant defects: First principles simulations of Se hyperdoped Si, Semicond. Sci. Technol. **38**, 014002 (2023).

[12] I. Umezu, J. M. Warrender, S. Charnvanichborikarn, A. Kohno, J. S. Williams, M. Tabbal, D. G. Papazoglou, X.-C. Zhang, and M. J. Aziz, Emergence of very broad infrared absorption band by hyperdoping of silicon with chalcogens, J. Appl. Phys. **113**, 213501 (2013).

[13] "In addition to point and line defects, there are defects which are composed of a small number of point defects. These are referred to as complexes," as stated in Ref. [27].

[14] A. Debernardi, Microscopic mechanisms driving the removal of electrical deactivation defects in Se ultra-doped silicon: An *ab initio* study. presented at EMRS 2022 Spring Meeting (unpublished).

[15] M. Fanciulli *et al.* (private communication); Electron spin resonance characterization of silicon hyper-doped with Te125, presented at EMRS 2022 Spring Meeting (unpublished).

[16] M. Hoesch, O. Fedchenko, M. Wang, C. Schlueter, D. Potorochin, K. Medjanik, S. Babenkov, A. S. Ciobanu, A. Winkelmann, H.-J. Elmers, S. Zhou, M. Helm, and G. Schönhense, Active sites of Te-hyperdoped silicon by hard x-ray photoelectron spectroscopy, Appl. Phys. Lett. **122**, 252108 (2023).

[17] H. Bracht, Self- and foreign-atom diffusion in semiconductor isotope heterostructures. I. Continuum theoretical calculations, Phys. Rev. B **75**, 035210 (2007).

[18] F. Rollert, N. A. Stolwijk, and H. Mehrer, Diffusion of sulfur-35 into silicon using an elemental vapor source, Appl. Phys. Lett. **63**, 506 (1993).

[19] Y. Mo, M. Z. Bazant, and E. Kaxiras, Sulfur point defects in crystalline and amorphous silicon, Phys. Rev. B **70**, 205210 (2004).

[20] The model can be trivially generalized to account for partial diffusion in the Λ_d shell, by substituting in $N_{\Lambda_d} \equiv \sum_{k=1}^{\Lambda_d} z_k$, z_{Λ_d} with a lesser value.

[21] D. C. Mueller and W. Fichtner, Highly *n*-doped silicon: Deactivating defects of donors, Phys. Rev. B **70**, 245207 (2004).

[22] This is Shorthand notation, analogous to the one used in the literature for As complexes, to denote the $(S_{Si})_n$-V_{Si} complex ($n = 1, 2, 3, 4$).

[23] See Supplemental Material at https://link.aps.org/supplemental/10.1103/y5zw-qt7d for additional computational details, the statistical model for sulfur-related complexes, the phenomenological estimate of the critical concentration, and extended infrared absorption spectra, which includes Refs. [27–39].

[24] The concentration at which the formation energy becomes almost constant, generally corresponds to the merging of the IB into the CB, denoted as $x_M(D)$. The exception is the monomer S_{Si}, whose formation energy becomes flat at concentration below $x_M(S_{Si})$.

[25] See Sec. B of the Supplemental Material [23].

[26] This effect can be explained, at least partially, by the fact that S has a smaller covalent radius and a deeper impurity band in the band gap of Si than the other chalcogens.

[27] P. Y. Yu and M. Cardona, *Fundamentals of Semiconductors* (Springer, Berlin, 2005).

[28] L. Cai, S. Wang, M. Huang, Y.-N. Wu, and S. Chen, First-principles identification of deep energy levels of sulfur impurities in silicon and their carrier capture cross sections, J. Phys. D **54**, 335103 (2021).

[29] P. Giannozzi, S. Baroni, N. Bonini, M. Calandra, R. Car, *et al.*, QUANTUM ESPRESSO: A modular and open-source software project for quantum simulations of materials, J. Phys.: Condens. Matter **21**, 395502 (2009).

[30] A. M. Rappe, K. M. Rabe, E. Kaxiras, and J. D. Joannopoulos, Optimized pseudopotentials, Phys. Rev. B **41**, 1227 (1990).

[31] D. Vanderbilt, Soft self-consistent pseudopotentials in a generalized eigenvalue formalism, Phys. Rev. B **41**, 7892 (1990).

[32] D. M. Bylander and L. Kleinman, Optimized effective potentials for semiconductors, Phys. Rev. B **52**, 14566 (1995).

[33] J. P. Perdew, K. Burke, and M. Ernzerhof, Generalized gradient approximation made simple, Phys. Rev. Lett. **77**, 3865 (1996).

[34] H. J. Monkhorst and J. D. Pack, Special points for Brillouin-zone integrations, Phys. Rev. B **13**, 5188 (1976).

[35] C. G. Broyden, The convergence of a class of double-rank minimization algorithms 1. general considerations, IMA J. Appl. Math. **6**, 76 (1970).

[36] A. Marini, C. Hogan, M. Grüning, and D. Varsano, Yambo: An *ab initio* tool for excited state calculations, Comput. Phys. Commun. **180**, 1392 (2009).

[37] F. Melone, First principles simulations of electronic and optical properties of S hyperdoped silicon, Master's thesis, University of Milano, 2024.

[38] J. Byrnes, *Unexploded Ordnance Detection and Mitigation* (Springer, Berlin, 2009).

[39] R. Paschotta, Infrared light, RP Photonics Encyclopedia, 2021, archived version retrieved 1 August 2021, https://www.rp-photonics.com/infrared_light.html.

[40] M. J. van Setten, M. Giantomassi, E. Bousquet, M. J. Verstraete, D. R. Hamann, X. Gonze, and G.-M. Rignanese, The PseudoDojo: Training and grading a 85 element optimized norm-conserving pseudopotential table, Comput. Phys. Commun. **226**, 39 (2018).